Search for charginos in e^+e^- interactions at $\sqrt{s} = 189$ GeV

DELPHI Collaboration

Abstract

An update of the searches for charginos and gravitinos is presented, based on a data sample corresponding to the 158 pb^{-1} recorded by the DELPHI detector in 1998, at a centre-of-mass energy of 189 GeV. No evidence for a signal was found. The lower mass limits are 4-5 GeV/c^2 higher than those obtained at a centre-of-mass energy of 183 GeV. The (μ,M$_2$) MSSM domain excluded by combining the chargino searches with neutralino searches at the Z resonance implies a limit on the mass of the lightest neutralino which, for a heavy sneutrino, is constrained to be above 31.0 GeV/c^2 for $\tan\beta \geq 1$.

arXiv:hep-ex/0104027v1 13 Apr 2001

P.Abreu[22], W.Adam[52], T.Adye[38], P.Adzic[12], I.Ajinenko[44], Z.Albrecht[18], T.Alderweireld[2], G.D.Alekseev[17], R.Alemany[51], T.Allmendinger[18], P.P.Allport[23], S.Almehed[25], U.Amaldi[9,29], N.Amapane[47], S.Amato[49], E.G.Anassontzis[3], P.Andersson[46], A.Andreazza[9], S.Andringa[22], P.Antilogus[26], W-D.Apel[18], Y.Arnoud[9], B.Åsman[46], J-E.Augustin[26], A.Augustinus[9], P.Baillon[9], P.Bambade[20], F.Barao[22], G.Barbiellini[48], R.Barbier[26], D.Y.Bardin[17], G.Barker[18], A.Baroncelli[40], M.Battaglia[16], M.Baubillier[24], K-H.Becks[54], M.Begalli[6], A.Behrmann[54], P.Beilliere[8], Yu.Belokopytov[9], N.C.Benekos[33], A.C.Benvenuti[5], C.Berat[15], M.Berggren[24], D.Bertrand[2], M.Besancon[41], M.Bigi[47], M.S.Bilenky[17], M-A.Bizouard[20], D.Bloch[10], H.M.Blom[32], M.Bonesini[29], M.Boonekamp[41], P.S.L.Booth[23], A.W.Borgland[4], G.Borisov[20], C.Bosio[43], O.Botner[50], E.Boudinov[32], B.Bouquet[20], C.Bourdarios[20], T.J.V.Bowcock[23], I.Boyko[17], I.Bozovic[12], M.Bozzo[14], M.Bracko[45], P.Branchini[40], R.A.Brenner[50], P.Bruckman[9], J-M.Brunet[8], L.Bugge[34], T.Buran[34], B.Buschbeck[52], P.Buschmann[54], S.Cabrera[51], M.Caccia[28], M.Calvi[29], T.Camporesi[9], V.Canale[39], F.Carena[9], L.Carroll[23], C.Caso[14], M.V.Castillo Gimenez[51], A.Cattai[9], F.R.Cavallo[5], V.Chabaud[9], Ph.Charpentier[9], P.Checchia[37], G.A.Chelkov[17], R.Chierici[47], P.Chliapnikov[9,44], P.Chochula[7], V.Chorowicz[26], J.Chudoba[31], K.Cieslik[19], P.Collins[9], R.Contri[14], E.Cortina[51], G.Cosme[20], F.Cossutti[9], H.B.Crawley[1], D.Crennell[38], S.Crepe[15], G.Crosetti[14], J.Cuevas Maestro[35], S.Czellar[16], M.Davenport[9], W.Da Silva[24], G.Della Ricca[48], P.Delpierre[27], N.Demaria[9], A.De Angelis[48], W.De Boer[18], C.De Clercq[2], B.De Lotto[48], A.De Min[37], L.De Paula[49], H.Dijkstra[9], L.Di Ciaccio[9,39], J.Dolbeau[8], K.Doroba[53], M.Dracos[10], J.Drees[54], M.Dris[33], A.Duperrin[26], J-D.Durand[9], G.Eigen[4], T.Ekelof[50], G.Ekspong[46], M.Ellert[50], M.Elsing[9], J-P.Engel[10], M.Espirito Santo[9], G.Fanourakis[12], D.Fassouliotis[12], J.Fayot[24], M.Feindt[18], A.Ferrer[51], E.Ferrer-Ribas[20], F.Ferro[14], S.Fichet[24], A.Firestone[1], U.Flagmeyer[54], H.Foeth[9], E.Fokitis[33], F.Fontanelli[14], B.Franek[38], A.G.Frodesen[4], R.Fruhwirth[52], F.Fulda-Quenzer[20], J.Fuster[51], A.Galloni[23], D.Gamba[47], S.Gamblin[20], M.Gandelman[49], C.Garcia[51], C.Gaspar[9], M.Gaspar[49], U.Gasparini[37], Ph.Gavillet[9], E.N.Gazis[33], D.Gele[10], T.Geralis[12], L.Gerdyukov[44], N.Ghodbane[26], I.Gil[51], F.Glege[54], R.Gokieli[9,53], B.Golob[9,45], G.Gomez-Ceballos[42], P.Goncalves[22], I.Gonzalez Caballero[42], G.Gopal[38], L.Gorn[1], Yu.Gouz[44], V.Gracco[14], J.Grahl[1], E.Graziani[40], P.Gris[41], G.Grosdidier[20], K.Grzelak[53], J.Guy[38], C.Haag[18], F.Hahn[9], S.Hahn[54], S.Haider[9], A.Hallgren[50], K.Hamacher[54], J.Hansen[34], F.J.Harris[36], V.Hedberg[9,25], S.Heising[18], J.J.Hernandez[51], P.Herquet[2], H.Herr[9], T.L.Hessing[36], J.-M.Heuser[54], E.Higon[51], S-O.Holmgren[46], P.J.Holt[36], S.Hoorelbeke[2], M.Houlden[23], J.Hrubec[52], M.Huber[18], K.Huet[2], G.J.Hughes[23], K.Hultqvist[9,46], J.N.Jackson[23], R.Jacobsson[9], P.Jalocha[19], R.Janik[7], Ch.Jarlskog[25], G.Jarlskog[25], P.Jarry[41], B.Jean-Marie[20], D.Jeans[36], E.K.Johansson[46], P.Jonsson[26], C.Joram[9], P.Juillot[10], L.Jungermann[18], F.Kapusta[24], K.Karafasoulis[12], S.Katsanevas[26], E.C.Katsoufis[33], R.Keranen[18], G.Kernel[45], B.P.Kersevan[45], Yu.Khokhlov[44], B.A.Khomenko[17], N.N.Khovanski[17], A.Kiiskinen[16], B.King[23], A.Kinvig[23], N.J.Kjaer[9], O.Klapp[54], H.Klein[9], P.Kluit[32], P.Kokkinias[12], V.Kostioukhine[44], C.Kourkoumelis[3], O.Kouznetsov[17], M.Krammer[52], E.Kriznic[45], Z.Krumstein[17], P.Kubinec[7], J.Kurowska[53], K.Kurvinen[16], J.W.Lamsa[1], D.W.Lane[1], J-P.Laugier[41], R.Lauhakangas[16], G.Leder[52], F.Ledroit[15], V.Lefebure[2], L.Leinonen[46], A.Leisos[12], R.Leitner[31], G.Lenzen[54], V.Lepeltier[20], T.Lesiak[19], M.Lethuillier[41], J.Libby[36], W.Liebig[54], D.Liko[9], A.Lipniacka[9,46], I.Lippi[37], B.Loerstad[25], J.G.Loken[36], J.H.Lopes[49], J.M.Lopez[42], R.Lopez-Fernandez[15], D.Loukas[12], P.Lutz[41], L.Lyons[36], J.MacNaughton[52], J.R.Mahon[6], A.Maio[22], A.Malek[54], T.G.M.Malmgren[46], S.Maltezos[33], V.Malychev[17], F.Mandl[52], J.Marco[42], R.Marco[42], B.Marechal[49], M.Margoni[37], J-C.Marin[9], C.Mariotti[9], A.Markou[12], C.Martinez-Rivero[20], F.Martinez-Vidal[51], S.Marti i Garcia[9], J.Masik[13], N.Mastroyiannopoulos[12], F.Matorras[42], C.Matteuzzi[29], G.Matthiae[39], F.Mazzucato[37], M.Mazzucato[37], M.Mc Cubbin[23], R.Mc Kay[1], R.Mc Nulty[23], G.Mc Pherson[23], C.Meroni[28], W.T.Meyer[1], E.Migliore[9], L.Mirabito[26], W.A.Mitaroff[52], U.Mjoernmark[25], T.Moa[46], M.Moch[18], R.Moeller[30], K.Moenig[9,11], M.R.Monge[14], D.Moraes[49], X.Moreau[24], P.Morettini[14], G.Morton[36], U.Mueller[54], K.Muenich[54], M.Mulders[32], C.Mulet-Marquis[15], R.Muresan[25], W.J.Murray[38], B.Muryn[19], G.Myatt[36], T.Myklebust[34], F.Naraghi[15], M.Nassiakou[12], F.L.Navarria[5], S.Navas[51], K.Nawrocki[53], P.Negri[29], N.Neufeld[9], R.Nicolaidou[41], B.S.Nielsen[30], P.Niezurawski[53], M.Nikolenko[10,17], V.Nomokonov[16], A.Nygren[25], V.Obraztsov[44], A.G.Olshevski[17], A.Onofre[22], R.Orava[16], G.Orazi[10], K.Osterberg[16], A.Ouraou[41], M.Paganoni[29], S.Paiano[5], R.Pain[24], R.Paiva[22], J.Palacios[36], H.Palka[19], Th.D.Papadopoulou[9,33], L.Pape[9], C.Parkes[9], F.Parodi[14], U.Parzefall[23], A.Passeri[40], O.Passon[54], T.Pavel[25], M.Pegoraro[37], L.Peralta[22], M.Pernicka[52], A.Perrotta[5], C.Petridou[48], A.Petrolini[14], H.T.Phillips[38], F.Pierre[41], M.Pimenta[22], E.Piotto[28], T.Podobnik[45], M.E.Pol[6], G.Polok[19], P.Poropat[48], V.Pozdniakov[17], P.Privitera[39], N.Pukhaeva[17], A.Pullia[29], D.Radojicic[36], S.Ragazzi[29], H.Rahmani[33], J.Rames[13], P.N.Ratoff[21], A.L.Read[34], P.Rebecchi[9], N.G.Redaelli[29], M.Regler[52], J.Rehn[18], D.Reid[32], R.Reinhardt[54], P.B.Renton[36], L.K.Resvanis[3], F.Richard[20], J.Ridky[13], G.Rinaudo[47], I.Ripp-Baudot[10], O.Rohne[34], A.Romero[47], P.Ronchese[37], E.I.Rosenberg[1], P.Rosinsky[7], P.Roudeau[20], T.Rovelli[5], Ch.Royon[41], V.Ruhlmann-Kleider[41], A.Ruiz[42], H.Saarikko[16], Y.Sacquin[41], A.Sadovsky[17], G.Sajot[15], J.Salt[51], D.Sampsonidis[12], M.Sannino[14], Ph.Schwemling[24], B.Schwering[54], U.Schwickerath[18], F.Scuri[48], P.Seager[21], Y.Sedykh[17], A.M.Segar[36], N.Seibert[18], R.Sekulin[38], R.C.Shellard[6], M.Siebel[54], L.Simard[41], F.Simonetto[37], A.N.Sisakian[17], G.Smadja[26], N.Smirnov[44], O.Smirnova[25], G.R.Smith[38], A.Sokolov[44], A.Sopczak[18], R.Sosnowski[53], T.Spassov[22], E.Spiriti[40], S.Squarcia[14], C.Stanescu[40], S.Stanic[45], M.Stanitzki[18], K.Stevenson[36], A.Stocchi[20], J.Strauss[52], R.Strub[10], B.Stugu[4], M.Szczekowski[53], M.Szeptycka[53], T.Tabarelli[29], A.Taffard[23], O.Tchikilev[44], F.Tegenfeldt[50], F.Terranova[29], J.Thomas[36], J.Timmermans[32], N.Tinti[5], L.G.Tkatchev[17], M.Tobin[23], S.Todorova[9], A.Tomaradze[2], B.Tome[22], A.Tonazzo[9], L.Tortora[40], P.Tortosa[51], G.Transtromer[25], D.Treille[9], G.Tristram[8], M.Trochimczuk[53], C.Troncon[28], M-L.Turluer[41],

I.A.Tyapkin[17], P.Tyapkin[25], S.Tzamarias[12], O.Ullaland[9], V.Uvarov[44], G.Valenti[9,5], E.Vallazza[48], C.Vander Velde[2], P.Van Dam[32], W.Van den Boeck[2], W.K.Van Doninck[2], J.Van Eldik[9,32], A.Van Lysebetten[2], N.van Remortel[2], I.Van Vulpen[32], G.Vegni[28], L.Ventura[37], W.Venus[38,9], F.Verbeure[2], P.Verdier[26], M.Verlato[37], L.S.Vertogradov[17], V.Verzi[28], D.Vilanova[41], L.Vitale[48], E.Vlasov[44], A.S.Vodopyanov[17], G.Voulgaris[3], V.Vrba[13], H.Wahlen[54], C.Walck[46], A.J.Washbrook[23], C.Weiser[9], D.Wicke[54], J.H.Wickens[2], G.R.Wilkinson[36], M.Winter[10], M.Witek[19], G.Wolf[9], J.Yi[1], O.Yushchenko[44], A.Zalewska[19], P.Zalewski[53], D.Zavrtanik[45], E.Zevgolatakos[12], N.I.Zimin[17,25], A.Zintchenko[17], Ph.Zoller[10], G.C.Zucchelli[46], G.Zumerle[37]

[1]Department of Physics and Astronomy, Iowa State University, Ames IA 50011-3160, USA
[2]Physics Department, Univ. Instelling Antwerpen, Universiteitsplein 1, B-2610 Antwerpen, Belgium
 and IIHE, ULB-VUB, Pleinlaan 2, B-1050 Brussels, Belgium
 and Faculté des Sciences, Univ. de l'Etat Mons, Av. Maistriau 19, B-7000 Mons, Belgium
[3]Physics Laboratory, University of Athens, Solonos Str. 104, GR-10680 Athens, Greece
[4]Department of Physics, University of Bergen, Allégaten 55, NO-5007 Bergen, Norway
[5]Dipartimento di Fisica, Università di Bologna and INFN, Via Irnerio 46, IT-40126 Bologna, Italy
[6]Centro Brasileiro de Pesquisas Físicas, rua Xavier Sigaud 150, BR-22290 Rio de Janeiro, Brazil
 and Depto. de Física, Pont. Univ. Católica, C.P. 38071 BR-22453 Rio de Janeiro, Brazil
 and Inst. de Física, Univ. Estadual do Rio de Janeiro, rua São Francisco Xavier 524, Rio de Janeiro, Brazil
[7]Comenius University, Faculty of Mathematics and Physics, Mlynska Dolina, SK-84215 Bratislava, Slovakia
[8]Collège de France, Lab. de Physique Corpusculaire, IN2P3-CNRS, FR-75231 Paris Cedex 05, France
[9]CERN, CH-1211 Geneva 23, Switzerland
[10]Institut de Recherches Subatomiques, IN2P3 - CNRS/ULP - BP20, FR-67037 Strasbourg Cedex, France
[11]Now at DESY-Zeuthen, Platanenallee 6, D-15735 Zeuthen, Germany
[12]Institute of Nuclear Physics, N.C.S.R. Demokritos, P.O. Box 60228, GR-15310 Athens, Greece
[13]FZU, Inst. of Phys. of the C.A.S. High Energy Physics Division, Na Slovance 2, CZ-180 40, Praha 8, Czech Republic
[14]Dipartimento di Fisica, Università di Genova and INFN, Via Dodecaneso 33, IT-16146 Genova, Italy
[15]Institut des Sciences Nucléaires, IN2P3-CNRS, Université de Grenoble 1, FR-38026 Grenoble Cedex, France
[16]Helsinki Institute of Physics, HIP, P.O. Box 9, FI-00014 Helsinki, Finland
[17]Joint Institute for Nuclear Research, Dubna, Head Post Office, P.O. Box 79, RU-101 000 Moscow, Russian Federation
[18]Institut für Experimentelle Kernphysik, Universität Karlsruhe, Postfach 6980, DE-76128 Karlsruhe, Germany
[19]Institute of Nuclear Physics and University of Mining and Metalurgy, Ul. Kawiory 26a, PL-30055 Krakow, Poland
[20]Université de Paris-Sud, Lab. de l'Accélérateur Linéaire, IN2P3-CNRS, Bât. 200, FR-91405 Orsay Cedex, France
[21]School of Physics and Chemistry, University of Lancaster, Lancaster LA1 4YB, UK
[22]LIP, IST, FCUL - Av. Elias Garcia, 14-1°, PT-1000 Lisboa Codex, Portugal
[23]Department of Physics, University of Liverpool, P.O. Box 147, Liverpool L69 3BX, UK
[24]LPNHE, IN2P3-CNRS, Univ. Paris VI et VII, Tour 33 (RdC), 4 place Jussieu, FR-75252 Paris Cedex 05, France
[25]Department of Physics, University of Lund, Sölvegatan 14, SE-223 63 Lund, Sweden
[26]Université Claude Bernard de Lyon, IPNL, IN2P3-CNRS, FR-69622 Villeurbanne Cedex, France
[27]Univ. d'Aix - Marseille II - CPP, IN2P3-CNRS, FR-13288 Marseille Cedex 09, France
[28]Dipartimento di Fisica, Università di Milano and INFN-MILANO, Via Celoria 16, IT-20133 Milan, Italy
[29]Dipartimento di Fisica, Univ. di Milano-Bicocca and INFN-MILANO, Piazza delle Scienze 2, IT-20126 Milan, Italy
[30]Niels Bohr Institute, Blegdamsvej 17, DK-2100 Copenhagen Ø, Denmark
[31]IPNP of MFF, Charles Univ., Areal MFF, V Holesovickach 2, CZ-180 00, Praha 8, Czech Republic
[32]NIKHEF, Postbus 41882, NL-1009 DB Amsterdam, The Netherlands
[33]National Technical University, Physics Department, Zografou Campus, GR-15773 Athens, Greece
[34]Physics Department, University of Oslo, Blindern, NO-1000 Oslo 3, Norway
[35]Dpto. Fisica, Univ. Oviedo, Avda. Calvo Sotelo s/n, ES-33007 Oviedo, Spain
[36]Department of Physics, University of Oxford, Keble Road, Oxford OX1 3RH, UK
[37]Dipartimento di Fisica, Università di Padova and INFN, Via Marzolo 8, IT-35131 Padua, Italy
[38]Rutherford Appleton Laboratory, Chilton, Didcot OX11 OQX, UK
[39]Dipartimento di Fisica, Università di Roma II and INFN, Tor Vergata, IT-00173 Rome, Italy
[40]Dipartimento di Fisica, Università di Roma III and INFN, Via della Vasca Navale 84, IT-00146 Rome, Italy
[41]DAPNIA/Service de Physique des Particules, CEA-Saclay, FR-91191 Gif-sur-Yvette Cedex, France
[42]Instituto de Fisica de Cantabria (CSIC-UC), Avda. los Castros s/n, ES-39006 Santander, Spain
[43]Dipartimento di Fisica, Università degli Studi di Roma La Sapienza, Piazzale Aldo Moro 2, IT-00185 Rome, Italy
[44]Inst. for High Energy Physics, Serpukov P.O. Box 35, Protvino, (Moscow Region), Russian Federation
[45]J. Stefan Institute, Jamova 39, SI-1000 Ljubljana, Slovenia and Laboratory for Astroparticle Physics,
 Nova Gorica Polytechnic, Kostanjeviska 16a, SI-5000 Nova Gorica, Slovenia,
 and Department of Physics, University of Ljubljana, SI-1000 Ljubljana, Slovenia
[46]Fysikum, Stockholm University, Box 6730, SE-113 85 Stockholm, Sweden
[47]Dipartimento di Fisica Sperimentale, Università di Torino and INFN, Via P. Giuria 1, IT-10125 Turin, Italy
[48]Dipartimento di Fisica, Università di Trieste and INFN, Via A. Valerio 2, IT-34127 Trieste, Italy
 and Istituto di Fisica, Università di Udine, IT-33100 Udine, Italy
[49]Univ. Federal do Rio de Janeiro, C.P. 68528 Cidade Univ., Ilha do Fundão BR-21945-970 Rio de Janeiro, Brazil
[50]Department of Radiation Sciences, University of Uppsala, P.O. Box 535, SE-751 21 Uppsala, Sweden
[51]IFIC, Valencia-CSIC, and D.F.A.M.N., U. de Valencia, Avda. Dr. Moliner 50, ES-46100 Burjassot (Valencia), Spain
[52]Institut für Hochenergiephysik, Österr. Akad. d. Wissensch., Nikolsdorfergasse 18, AT-1050 Vienna, Austria
[53]Inst. Nuclear Studies and University of Warsaw, Ul. Hoza 69, PL-00681 Warsaw, Poland
[54]Fachbereich Physik, University of Wuppertal, Postfach 100 127, DE-42097 Wuppertal, Germany

1 Introduction

In 1998, the LEP centre-of-mass energy reached 189 GeV, and the DELPHI experiment collected an integrated luminosity of 158 pb^{-1}. These data have been analysed to search for charginos, supersymmetric partners of Higgs and gauge bosons, predicted by supersymmetric (SUSY) models [1].

A description of the parts of the DELPHI detector relevant to the present paper can be found in [2], while a complete description is given in [3].

The results obtained at the same centre-of-mass energy by other LEP collaborations, on similar searches, are described in [4].

The conservation of R-parity, implying a stable lightest supersymmetric particle (LSP), is assumed. This also means that charginos are pair produced in e$^+$e$^-$ collisions. The analysis was performed in the framework of the Minimal Supersymmetric extension of the Standard Model (MSSM), with universal parameters at the high mass scale typical of Grand Unified Theories (GUT's) [1]. The parameters of this model relevant to the present searches are the masses M_1 and M_2 of the gaugino sector (which are assumed to satisfy the GUT relation $M_1 = \frac{5}{3}\tan^2\theta_W M_2 \approx 0.5M_2$ at the electroweak scale), the universal mass m_0 of the scalar fermion sector, the Higgs mass parameter μ, and the ratio $\tan\beta$ of the vacuum expectation values of the two Higgs doublets. In this paper it is assumed that $m_0 =1$ TeV. Scalar mass unification is assumed, except for the sneutrino mass which is considered to be a free parameter. As in Ref. [2] both cases where either the lightest neutralino ($\tilde{\chi}_1^0$) or the gravitino ($\tilde{G}$) is the LSP are considered.

In the former case, the decay of the charginos is $\tilde{\chi}_1^\pm \to \tilde{\chi}_1^0 f\bar{f}'$ (f$\bar{f}'$ can be quarks or leptons) and the events are characterised by missing energy carried by the escaping $\tilde{\chi}_1^0$. In some areas of the parameter space, the charginos can decay to heavier neutralinos giving rise to a cascade effect: $\tilde{\chi}_1^\pm \to \tilde{\chi}_2^0 f_1\bar{f}_1' \to \tilde{\chi}_1^0\ f_1\bar{f}_1'\ f_2\bar{f}_2$ (f$_1\bar{f}_1'$ f$_2\bar{f}_2$ can be quarks or leptons). The decay $\tilde{\chi}_2^0 \to \tilde{\chi}_1^0\gamma$ may occur for small $\mu \approx -M_2$. So the following decay channels were defined:

- The *leptonic* channel ($\ell\ell$): the decay products are only leptons and the LSPs.
- The *hadronic* channel (*jets*): the decay products are only quarks and the LSPs.
- The *semi-leptonic* channel ($jj\ell$): the decay products are quarks, leptons and the LSPs.
- The *radiative* channel (*rad*): there is at least one isolated photon among the decay products.

In this scenario the likelihood ratio method [5] was used to optimize the search for charginos. An overview of this method and details of the implementation are given in 3.1.

If the gravitino is the LSP, the decay $\tilde{\chi}_1^0 \to \tilde{G}\gamma$ is possible [6,7,8]. If the gravitino is sufficiently light (with a mass below about 10 eV/c^2 [8]), this decay takes place within the detector. As gravitinos escape detection, the typical signature of these SUSY events is missing energy and isolated photons. The selection criteria already used at a centre-of-mass energy of 183 GeV are applied in this scenario. The detailed description of the analysis can be found in Ref. [2].

2 Event generators

To evaluate the signal efficiencies and background contaminations, events were generated using several different programs. All relied on JETSET 7.4 [9], tuned to LEP 1 data [10], for quark fragmentation.

The program `SUSYGEN` [11] was used to generate events with chargino production and decay in both the neutralino LSP and the gravitino LSP scenarios, and to calculate masses, cross-sections and branching ratios for each adopted parameter set. These agree with the calculations of Ref. [12]. Details of the signal samples generated are given in section 4.

The background process $e^+e^- \to q\bar{q}(n\gamma)$ was generated with `PYTHIA 5.7` [9], while `DYMU3` [13] and `KORALZ 4.2` [14] were used for $\mu^+\mu^-(\gamma)$ and $\tau^+\tau^-(\gamma)$, respectively. The generator of Ref. [15] was used for $e^+e^- \to e^+e^-$ events. Processes leading to four-fermion final states, $(Z/\gamma)^*(Z/\gamma)^*$, W^+W^-, $We\nu_e$ and Ze^+e^-, were generated using `EXCALIBUR` [16] and `GRC4F` [17].

Two-photon interactions leading to hadronic final states were generated using `TWOGAM` [18], separating the VDM (Vector Dominance Model) and QCD components. The generators of Berends, Daverveldt and Kleiss [19] were used for the QPM (Quark Parton Model) component and for leptonic final states.

The generated signal and background events were passed through the detailed simulation of the DELPHI detector [3] and then processed with the same reconstruction and analysis programs as real data events. The number of simulated events from different background processes was several times (a factor varying from 2 to 140 depending on the background process) the number of real events recorded.

3 Event selections

The criteria used to select events were defined on the basis of the simulated signal and background events. The selections for charged and neutral particles were similar to those presented in [2], requiring charged particles to have momentum above 100 MeV/c and to extrapolate back to within 5 cm of the main vertex in the transverse plane, and to within twice this distance in the longitudinal direction. Calorimeter energy clusters above 100 MeV were taken as neutral particles if not associated to any charged particle track. The particle selection was followed by different event selections for the different signal topologies considered in the application of the likelihood ratio method, which was used in the stable $\tilde{\chi}_1^0$ case. The detailed description of the analysis done in the unstable $\tilde{\chi}_1^0$ case can be found in Ref. [2].

3.1 The likelihood ratio method

In the likelihood ratio method used, several discriminating variables are combined into one on the basis of their one-dimensional probability density functions (pdf). If the variables used are independent, this gives the best possible background suppression for a given signal efficiency [5]. For a set of variables $\{x_i\}$, the pdfs of these variables are estimated by normalised frequency distributions for the signal and the background samples. We denote the pdfs of these variables $f_i^S(x_i)$ for the signal events and $f_i^B(x_i)$ for the background events submitted to the same selection criteria. The likelihood ratio function is defined as $\mathcal{L}_\mathcal{R} = \prod_{i=1}^{n} \frac{f_i^S(x_i)}{f_i^B(x_i)}$. Events with $\mathcal{L}_\mathcal{R} > \mathcal{L}_{\mathcal{R}_{CUT}}$ are selected as candidate signal events. The optimal set of variables and the value of $\mathcal{L}_{\mathcal{R}_{CUT}}$ were defined in order to minimise the excluded cross-section expected in the absence of a signal (at 95% confidence level). The variables $\{x_i\}$ used to build the $\mathcal{L}_\mathcal{R}$ functions in the present analysis were [20]: the visible energy (E_{vis}), visible mass (M_{vis}), missing transverse momentum (p_T^{miss}), polar angle of the missing momentum, number of charged particles, total number

of particles, acoplanarity, acollinearity, ratio of electromagnetic energy to total energy, percentage of total energy within 30° of the beam axis, kinematic information concerning the isolated photons, leptons and two most energetic charged particles and finally the jet characteristics.

3.2 Chargino analysis

The signal and background events were divided into four mutually exclusive topologies:

- The $\ell\ell$ topology with no more than five charged particles and no isolated photons.
- The $jj\ell$ topology with more than five charged particles and at least one isolated lepton and no isolated photons.
- The *jets* topology with more than five charged particles and no isolated photons or leptons.
- The *rad* topology with at least one isolated photon.

The events in a given topology are mostly events of the corresponding decay channel, but events from other channels may also contribute. For instance, for low mass difference, ΔM, between the chargino and the lightest neutralino (and thus low visible energy) some events with hadronic decays are selected in the leptonic topology, and some mixed decay events with the isolated lepton unidentified enter into the hadronic topology. This migration effect tends to disappear as ΔM increases. This effect was taken into account in the final efficiency and limit computations.

The properties of the chargino decay products are mainly governed by the ΔM value. For low ΔM, the signal events are similar to $\gamma\gamma$ events, for high ΔM to four-fermion final states (W$^+$W$^-$, ZZ,..) while for intermediate ΔM values, the background is composed of many SM processes in comparable proportions.

The signal events were simulated for 76 combinations of $\tilde{\chi}_1^\pm$ and $\tilde{\chi}_1^0$ masses for five chargino mass values ($M_{\tilde{\chi}_1^\pm} \approx$ 94, 85, 70, 50 and 45 GeV/c^2) and with ΔM ranging from 3 GeV/c^2 to 70 GeV/c^2. A total of 152000 chargino events (2000 per combination) was generated and passed through the complete simulation of the DELPHI detector. The kinematic properties (acoplanarity, E_{vis}, p_T^{miss},..) of the signal events were studied in terms of their mean value and standard deviation, and six ΔM regions were defined in order to have signal events with similar properties (table 1).

In each of these 24 windows (four topologies, six ΔM regions), a likelihood ratio function was defined. The generation of these 24 functions was performed in five steps:

- The signal distributions of all the variables used in this analysis (see section 3.1) were built with signal events generated with parameter sets giving rise to charginos and neutralinos with masses in the corresponding ΔM region. For each ΔM region the events were classified according to the above topological cuts. The background distributions were built with background events passing the same topological cuts.
- Different preselection cuts, for each ΔM region, were applied in order to reduce the high cross-section backgrounds (two-photon interactions and Bhabha events) and to generate the pdfs. Fig. 1.a shows the distribution of the visible energy for $\Delta M >$ 50 GeV/c^2 in the $\ell\ell$ topology for real and simulated events. The agreement is satisfactory, the normalization is absolute. The pdfs were then generated as mentioned in 3.1.
- Then, to reduce statistical fluctuations a smoothing was performed by passing the 24 sets of pdfs for signal and background through a triangular filter [21].

- In each window all the combinations of the pdfs were tested, starting from a minimal set of four variables. Every combination defined a $\mathcal{L_R}$ function (see section 3.1) and a $\mathcal{L_{R_{CUT}}}$ computed in order to have the minimal expected excluded cross-section at 95% C.L. (Fig. 1.b) using the monochannel Bayesian formula [22]. The parameters entering this computation were the number of expected background events and the efficiency of the chargino selection. The efficiency of the chargino selection was defined in this case, as the number of events satisfying $\mathcal{L_R} > \mathcal{L_{R_{CUT}}}$ divided by the total number of chargino events satisfying the topological cuts. Fig. 1.c shows the dependence of the optimum likelihood ratio cut on the integrated luminosity, which demonstrates the importance of adjusting the cut to the luminosity. Fig. 1.d shows the good agreement obtained between real and simulated events as a function of the likelihood ratio cut, for $35 \leq \Delta M < 50 \text{ GeV}/c^2$ in the $jj\ell$ topology.
- The combination of variables corresponding to the lowest excluded cross-section defined the $\mathcal{L_R}$ function and the $\mathcal{L_{R_{CUT}}}$ of this window.

Finally, the selection to be applied for SUSY models with ΔM inside one such window was defined as a logical OR of the criteria for several windows, chosen to minimise the excluded cross-section expected in the absence of a signal [20].

	ΔM regions
1	$3 \leq \Delta M < 5 \text{ GeV}/c^2$
2	$5 \leq \Delta M < 10 \text{ GeV}/c^2$
3	$10 \leq \Delta M < 25 \text{ GeV}/c^2$
4	$25 \leq \Delta M < 35 \text{ GeV}/c^2$
5	$35 \leq \Delta M < 50 \text{ GeV}/c^2$
6	$50 \text{ GeV}/c^2 \leq \Delta M$

Table 1: Definitions of the ΔM regions.

4 Results

4.1 Stable $\tilde{\chi}_1^0$ case

4.1.1 Efficiencies and selected events

The total number of background events expected in the different topologies is shown in table 2, together with the number of events selected in the data.

The efficiencies of the chargino selection in the four topologies were computed separately for the 76 MSSM points using the $\mathcal{L_R}$ function and the $\mathcal{L_{R_{CUT}}}$ of the corresponding topology and ΔM region. To pass from the efficiencies of the chargino selection in the four topologies to the efficiencies in the four decay channels, all the migration effects were computed for all the generated points of the signal simulation. Then the efficiencies of the selection in the four decay channels were interpolated in the $(M_{\tilde{\chi}_1^\pm}, M_{\tilde{\chi}_1^0})$ plane using the same method as in Ref. [2]. When the interpolation was not possible (for $M_{\tilde{\chi}_1^\pm} \sim 80 \text{ GeV}/c^2$ and $M_{\tilde{\chi}_1^0} \sim 0 \text{ GeV}/c^2$) an extrapolation was used. These efficiencies as functions of $M_{\tilde{\chi}_1^\pm}$ and $M_{\tilde{\chi}_1^0}$ are shown in Fig. 2.

All the selected events in the real data are compatible with the expectation from the background simulation. As no evidence for a signal is found, exclusion limits are set at

Stable $\tilde{\chi}_1^0$

Topology:	$jj\ell$	$\ell\ell$	$jets$	rad	Total
	$3 \le \Delta M < 5$ GeV/c^2				
Obs. events:	0	46	1	4	51
Expect. events:	0.26 $^{+1.55}_{-0.07}$	43.2 $^{+3.7}_{-2.4}$	0.81 $^{+1.6}_{-0.13}$	2.85 $^{+1.61}_{-0.32}$	47.1 $^{+4.6}_{-2.4}$
	$5 \le \Delta M < 10$ GeV/c^2				
Obs. events:	0	14	4	4	22
Expect. events:	0.26 $^{+1.55}_{-0.07}$	14.3 $^{+2.5}_{-1.2}$	2.27 $^{+1.81}_{-0.29}$	2.85 $^{+1.61}_{-0.32}$	19.7 $^{+3.8}_{-1.2}$
	$10 \le \Delta M < 25$ GeV/c^2				
Obs. events:	0	25	9	4	38
Expect. events:	0.48 $^{+1.55}_{-0.08}$	25.2 $^{+2.7}_{-1.4}$	5.36 $^{+1.97}_{-0.49}$	2.85 $^{+1.61}_{-0.32}$	33.9 $^{+4.0}_{-1.6}$
	$25 \le \Delta M < 35$ GeV/c^2				
Obs. events:	0	11	4	4	19
Expect. events:	0.26 $^{+1.52}_{-0.05}$	13.0 $^{+2.0}_{-0.8}$	5.81 $^{+1.59}_{-0.37}$	2.85 $^{+1.61}_{-0.32}$	21.9 $^{+3.4}_{-0.9}$
	$35 \le \Delta M < 50$ GeV/c^2				
Obs. events:	0	24	21	2	47
Expect. events:	0.94 $^{+1.53}_{-0.14}$	25.8 $^{+2.6}_{-1.1}$	17.5 $^{+1.7}_{-0.7}$	1.71 $^{+1.56}_{-0.19}$	45.9 $^{+3.6}_{-1.4}$
	50 GeV/$c^2 \le \Delta M$				
Obs. events:	1	24	27	2	54
Expect. events:	1.32 $^{+1.56}_{-0.17}$	19.7 $^{+2.0}_{-0.9}$	21.8 $^{+1.9}_{-0.8}$	1.71 $^{+1.56}_{-0.19}$	44.8 $^{+3.5}_{-1.2}$
	TOTAL (logical OR between different ΔM windows)				
Obs. events:	1	70	36	5	112
Expect. events:	1.32 $^{+1.56}_{-0.17}$	66.7 $^{+3.9}_{-2.7}$	25.6 $^{+2.2}_{-1.0}$	3.57 $^{+1.63}_{-0.37}$	97.2 $^{+5.0}_{-2.9}$

Table 2: The number of events observed in data and the expected number of background events in the different chargino search topologies under the hypothesis of a stable $\tilde{\chi}_1^0$ (section 3.2).

95% C.L. using the multichannel Bayesian formula [22] taking into account the branching ratio and the efficiency of each decay channel.

4.1.2 Limits

Limits on chargino production

The simulated points were used to parametrize the efficiencies of the chargino selection criteria described in section 3.2 in terms of ΔM and the mass of the chargino (see section 4.1.1). Then a large number of SUSY points were investigated and the values of ΔM, the chargino and neutralino masses and the various decay branching ratios were determined for each point. By applying the appropriate efficiency (from the interpolation) and branching ratios and cross-sections for each channel decay (computed by SUSYGEN), the number of expected signal events can be calculated. Taking into account the expected background and the number of observed events, the corresponding point in the MSSM parameter space (μ, M_2, $\tan\beta$) can be excluded if the number of expected signal events is greater than the upper limit at 95% C.L. on the number of observed events of the corresponding ΔM region.

Fig. 3 shows the chargino production cross-sections as obtained in the MSSM at $\sqrt{s} = 189$ GeV for different chargino masses for the non-degenerate ($\Delta M > 10$ GeV/c^2) and degenerate cases ($\Delta M = 3$ GeV/c^2). The parameters M_2 and μ were varied randomly in the ranges 0 GeV/$c^2 < M_2 < 3000$ GeV/c^2 and -200 GeV/$c^2 < \mu < 200$ GeV/c^2 for three fixed different values of $\tan\beta$, namely 1, 1.5 and 35. The random generation of the parameters led to an accuracy on the mass limit computation of the order of 10 MeV/c^2. Two different cases were considered for the sneutrino mass: $M_{\tilde{\nu}} > 300$ GeV/c^2 (in the non-degenerate case) and $M_{\tilde{\nu}} > M_{\tilde{\chi}_1^\pm}$ (in the degenerate case).

To derive the chargino mass limits, constraints on the process $Z \to \tilde{\chi}_1^0 \tilde{\chi}_2^0 \to \tilde{\chi}_1^0 \tilde{\chi}_1^0 \gamma$ were also included. These were derived from the DELPHI results on single-photon production at LEP 1 [23].

The chargino mass limits are summarized in Table 3. The table also gives, for each case, the minimal MSSM cross-section for which $M_{\tilde{\chi}_1^\pm}$ is below the corresponding mass limit. These cross-section values are also displayed in Fig. 3. The chargino mass limits versus ΔM and versus M_2, assuming a heavy sneutrino, are shown in Figs. 4 and 5, respectively. The behaviour of the curve in Fig. 4 depends very weakly on the relation between M_1 and M_2. Note that in Fig. 5, for a fixed high value of M_2, the chargino mass limit is lower for positive μ than for negative μ. This is due to higher degeneracy for positive μ than for negative μ, for a fixed value of M_2.

In the non-degenerate case ($\Delta M > 10$ GeV/c^2) with a large sneutrino mass (> 300 GeV/c^2), the lower limit for the chargino ranges between 93.9 GeV/c^2 (for a mostly higgsino-like chargino) and 94.2 GeV/c^2 (for a mostly wino-like chargino). The minimal excluded MSSM cross-section at $\sqrt{s} = 189$ GeV is 0.23 pb, deriving from a chargino mass limit of 93.9 GeV/c^2. For $\Delta M > 20$ GeV/c^2, the lower limit for the chargino mass ranges between 94.1 GeV/c^2 and 94.2 GeV/c^2. In this case the minimum excluded MSSM cross-section at $\sqrt{s} = 189$ GeV is 0.13 pb.

In the degenerate case ($\Delta M = 3$ GeV/c^2), the cross-section does not depend significantly on the sneutrino mass, since the chargino is higgsino-like under the assumption of gaugino mass unification. The lower limit for the chargino mass, shown in Fig. 3, is 88.4 GeV/c^2. The minimal excluded cross-section is in this case 1.42 pb.

The systematic error on the given mass limits is less than 0.5% for $\Delta M = 3$ GeV/c^2 and less than 0.1% for $\Delta M > 20$ GeV/c^2.

Case	$m_{\tilde{\nu}}$	$M_{\chi^\pm}^{min}$	σ^{max}	N$_{95\%}$
	(GeV/c^2)	(GeV/c^2)	(pb)	
Stable $\tilde{\chi}_1^0$				
$\Delta M > 20$ GeV/c^2	> 300	94.1	0.13	10.6
$\Delta M > 10$ GeV/c^2	> 300	93.9	0.23	13.2
$\Delta M = 3$ GeV/c^2	> $M_{\tilde{\chi}_1^\pm}$	88.4	1.42	12.3
Unstable $\tilde{\chi}_1^0$				
$\Delta M > 10$ GeV/c^2	> 300	94.1	0.11	8.6
$\Delta M = 1$ GeV/c^2	> $M_{\tilde{\chi}_1^\pm}$	94.2	0.08	7.1

Table 3: 95% confidence level lower limits for the chargino mass, the corresponding pair production cross-sections at 189 GeV and the 95% confidence level upper limit on number of observed events, for the non-degenerate and a highly degenerate cases. The scenarios of a stable $\tilde{\chi}_1^0$ and $\tilde{\chi}_1^0 \to \tilde{G}\gamma$ are considered.

Limits on MSSM parameters and neutralino mass

The exclusion regions in the (μ, M_2) plane for $\tan\beta = 1$, 1.5 and 35 are shown in Fig. 6.a, 6.b, and 6.c, assuming a heavy sneutrino ($m_{\tilde{\nu}}>$ 300 GeV/c^2). These limits, based on data taken at $\sqrt{s} =$189 GeV, improve on previous limits at lower energies, and represent a significant increase in range as compared to LEP 1 results [24].

DELPHI limits on the process Z $\to \tilde{\chi}_1^0\tilde{\chi}_2^0 \to \tilde{\chi}_1^0\tilde{\chi}_1^0\gamma$ were derived from the single-photon search at LEP 1 [23]. These limits marginally extends part of the region covered by the chargino search at low $\tan\beta$ for small M_2 and negative μ (Fig. 6.d). The exclusion region obtained depends strongly on the the assumed GUT relation between M_1 and M_2.

The exclusion regions in the (μ, M_2) plane can be translated into a limit on the mass of the lightest neutralino also shown in the $(M_{\tilde{\chi}_1^\pm}, M_{\tilde{\chi}_1^0})$-plane in Fig. 7. A lower limit of 31.0 GeV/c^2 on the lighest neutralino mass is obtained, valid for $\tan\beta \geq 1$ and a heavy sneutrino. This limit is reached for $\tan\beta = 1$, $\mu = -57.8$ GeV/c^2, M$_2 = 52.05$ GeV/c^2. The small excluded region outside the chargino kinematic limit in Fig. 7 derives from the single-photon search at LEP 1 [23]. In the same figure, the vertical dotted line (partly hidden by the shading) shows the expected exclusion limit.

4.2 Unstable $\tilde{\chi}_1^0$ case

4.2.1 Efficiencies and selected events

The efficiency of the chargino selection for an unstable $\tilde{\chi}_1^0$ decaying into a photon and a gravitino was calculated from a total of 78000 events generated using the same combinations of $M_{\tilde{\chi}_1^\pm}$ and $M_{\tilde{\chi}_1^0}$ as in the stable $\tilde{\chi}_1^0$ scenario. As mentioned in [2], the same selection applies to all topologies. The efficiency, as shown in Fig. 8, varies only weakly with ΔM so only three ΔM windows were used in this case. Note that, due to the presence of the photons from the neutralino decay, the region of high degeneracy (down to $\Delta M = 1$ GeV/c^2) is fully covered.

The total number of background events expected in the three different ΔM ranges is shown in table 4, together with the number of events selected in the data. 24 events were found in the data, with a total expected background of 19.9 $\pm$1.9. Since no evidence for a signal was found, exclusion limits were set.

4.2.2 Limits

The chargino cross-section limits corresponding to the case where the neutralino is unstable and decays via $\tilde{\chi}_1^0 \to \tilde{G}\gamma$ were computed as explained in section 4.1.2 and are shown in Fig. 3 and in table 3. In the non-degenerate case the chargino mass limit at 95% C.L. is 94.1 GeV/c^2 for a heavy sneutrino, while in the ultra-degenerate case ($\Delta M = 1$ GeV/c^2) the limit is 94.2 GeV/c^2. The minimal MSSM cross-sections excluded by the above mass limits are 0.109 pb in the non-degenerate case and 0.081 pb in the ultra-degenerate case.

Unstable $\tilde{\chi}_1^0$

	$\Delta M > 10$ GeV/c^2	$5 \leq \Delta M \leq 10$ GeV/c^2	$\Delta M < 5$ GeV/c^2
Obs. events:	14	6	4
Expect. events:	15.1 $^{+1.8}_{-0.8}$	2.6 $^{+1.77}_{-0.32}$	2.2 $^{+1.73}_{-0.26}$

Table 4: The number of events observed and the expected number of background events in the different ΔM cases under the hypothesis of an unstable $\tilde{\chi}_1^0$ (section 3.2).

5 Summary

Searches for charginos at $\sqrt{s} = 189$ GeV allow the exclusion of a large domain of SUSY parameters, cross-sections, and masses, at 95% confidence level.

Assuming a difference in mass between chargino and neutralino, ΔM, of 10 GeV/c^2 or more, and a sneutrino heavier than 300 GeV/c^2, the existence of a chargino lighter than 93.9 GeV/c^2 can be excluded. If a gaugino-dominated chargino is assumed in addition, the kinematic limit is reached. If ΔM is 3 GeV/c^2, the lower limit on the chargino mass becomes 88.4 GeV/c^2, assuming a sneutrino heavier than the chargino.

A lower limit of 31.0 GeV/c^2 on the lightest neutralino mass is obtained assuming a heavy sneutrino and $M_1/M_2 \approx 0.5$, using the obtained chargino exclusion regions and including DELPHI results [23] on the process $Z \to \tilde{\chi}_1^0 \tilde{\chi}_2^0 \to \tilde{\chi}_1^0 \tilde{\chi}_1^0 \gamma$.

A specific $\tilde{\chi}_1^+ \tilde{\chi}_1^-$ production search was performed assuming the decay of the lightest neutralino into a photon and a gravitino, giving somewhat more stringent limits on cross-sections and masses than in the case of a stable $\tilde{\chi}_1^0$: $M_{\tilde{\chi}_1^\pm} > 94.1$ GeV/c^2 for large ΔM and $M_{\tilde{\chi}_1^\pm} > 94.2$ GeV/c^2 for $\Delta M = 1$ GeV/c^2.

Acknowledgements

References

[1] P. Fayet and S. Ferrara, Phys. Rep. **32** (1977) 249;
H.P. Nilles, Phys. Rep. **110** (1984) 1;
H.E. Haber and G.L. Kane, Phys. Rep. **117** (1985) 75.

[2] DELPHI Coll., P. Abreu *et al.*, Eur. Phys. J. **C1** (1998) 1-20.

[3] DELPHI Coll., P. Aarnio *et al.*, Nucl. Instr. and Meth. **303** (1991) 233;
DELPHI Coll., P. Abreu *et al.*, Nucl. Instr. and Meth. **378** (1996) 57.

[4] L3 Coll., M. Acciarri *et al.*,CERN-EP/99-127, Phys. Lett. **B472** (2000) 420;
OPAL Coll., G. Abbiendi *et al.*, CERN-EP/99-123, submitted to Eur. Phys. J. C.

[5] T.W. Anderson, An Introduction to multivariate analysis, New York Wiley, 1958.

[6] D. Dicus *et al.*, Phys. Rev. **D41** (1990) 2347;
D. Dicus *et al.*, Phys. Rev. **D43** (1991) 2951;
D. Dicus *et al.*, Phys. Lett. **B258** (1991) 231.

[7] S. Dimopoulos *et al.*, Phys. Rev. Lett. **76** (1996) 3494;
S. Ambrosanio *et al.*, Phys. Rev. Lett. **76** (1996) 3498;
J.L. Lopez and D.V. Nanopoulos, Mod. Phys. Lett. **A10** (1996) 2473;
J.L. Lopez and D.V. Nanopoulos, Phys. Rev. **D55** (1997) 4450.

[8] S. Ambrosanio *et al.*, Phys. Rev. **D54** (1996) 5395.

[9] T. Sjöstrand, Comp. Phys. Comm. **39** (1986) 347;
T. Sjöstrand, `PYTHIA 5.6` *and* `JETSET 7.3`, CERN-TH/6488-92.

[10] DELPHI Coll., P. Abreu *et al.*, Z. Phys. **C73** (1996) 11.

[11] S. Katsanevas and P. Morawitz, Comp. Phys. Comm. **112** (1998) 227.

[12] S. Ambrosanio and B. Mele, Phys. Rev. **D52** (1995) 3900;
S. Ambrosanio and B. Mele, Phys. Rev. **D53** (1996) 2451.

[13] J.E. Campagne and R. Zitoun, Z. Phys. **C43** (1989) 469.

[14] S. Jadach, B.F.L. Ward and Z. Was, Comp. Phys. Comm. **79** (1994) 503.

[15] F.A. Berends, R. Kleiss, W. Hollik, Nucl. Phys. **B304** (1988) 712.

[16] F.A. Berends, R. Pittau, R. Kleiss, Comp. Phys. Comm. **85** (1995) 437.

[17] J.Fujimoto *et al.*, Comp. Phys. Comm. **100** (1997) 128

[18] S. Nova, A. Olshevski, and T. Todorov, *A Monte Carlo event generator for two photon physics*, DELPHI note 90-35 (1990).

[19] F.A. Berends, P.H. Daverveldt, R. Kleiss, Comp. Phys. Comm. **40** (1986) 271, Comp. Phys. Comm. **40** (1986) 285, Comp. Phys. Comm. **40** (1986) 309.

[20] T. Alderweireld, I. Gil, P. Rebecchi, *Review of the chargino search in DELPHI. Latest results at $E_{\rm cm}$ = 189 GeV*, DELPHI note 99-177 PHYS 843 (1999).

[21] A.V. Oppenheim and R.W. Schafer, Discrete-time signal processing, Prentice-Hall, 1989

[22] V.F. Obraztsov, Nucl. Instr. and Meth. **316** (1992) 388;
V.F. Obraztsov, Nucl. Instr. and Meth. **399** (1997) 500.

[23] DELPHI Coll., P. Abreu *et al.*, Z. Phys. **C74** (1997) 577

[24] ALEPH Coll., D. Decamp *et al.*, Phys. Rep. **216** (1992) 253;
L3 Coll., M. Acciarri *et al.*, Phys. Lett. **B350** (1995) 109;
OPAL Coll., G. Alexander *et al.*, Phys. Lett. **B377** (1996) 273.
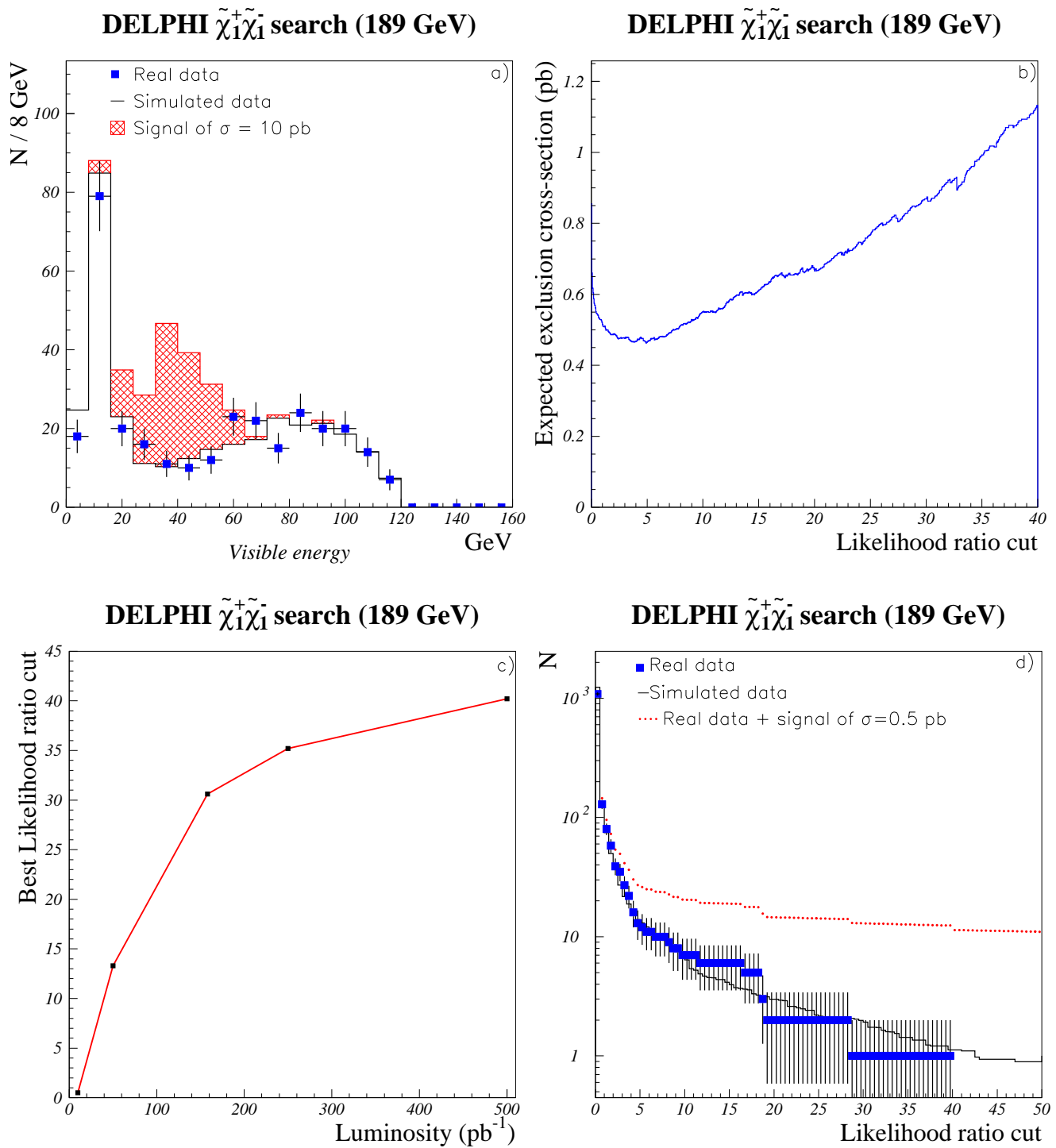
DELPHI $\tilde{\chi}_1^+\tilde{\chi}_1^-$ search (189 GeV)

Figure 1: a) comparison between real data (squares), simulated background events (histogram) and a possible chargino signal, $M_{\tilde{\chi}_1^\pm}$=94 GeV/c^2 $M_{\tilde{\chi}_1^0}$=40 GeV/c^2, of 10 pb (hatched) at the preselection level and b) choice of the best likelihood ratio cut for $\Delta M > 50$ GeV/c^2 in the $\ell\ell$ topology. The dependence of the optimum likelihood ratio cut as a function of the luminosity is shown in c) and the good agreement between real (squares) and simulated (histogram) events as a function of the likelihood ratio cut is shown in d), for $35 \leq \Delta M < 50$ GeV/c^2 in the $jj\ell$ topology. A possible signal, $M_{\tilde{\chi}_1^\pm}$=94 GeV/c^2 $M_{\tilde{\chi}_1^0}$=54 GeV/c^2, of 0.5 pb added to real data is shown in figure d) by the dotted curve.
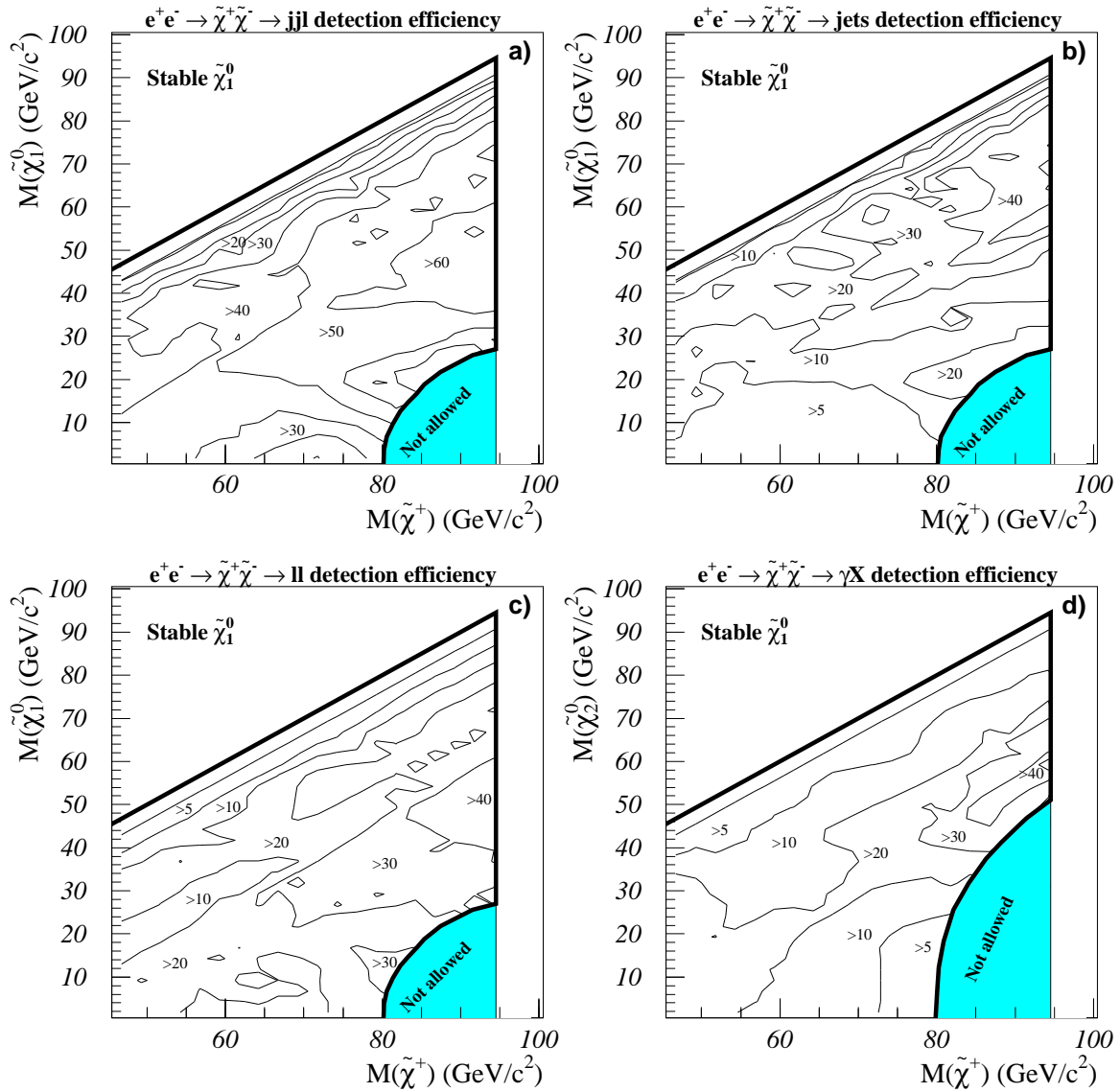
Figure 2: Chargino pair production detection efficiencies (%) for the four decay channels a) $jj\ell$, b) *jets*, c) $\ell\ell$ and d) *rad*, at 189 GeV in the $(M_{\tilde\chi^\pm}, M_{\tilde\chi^0})$ plane. A stable $\tilde\chi_1^0$ is assumed. The shaded areas are disallowed in the MSSM scheme.
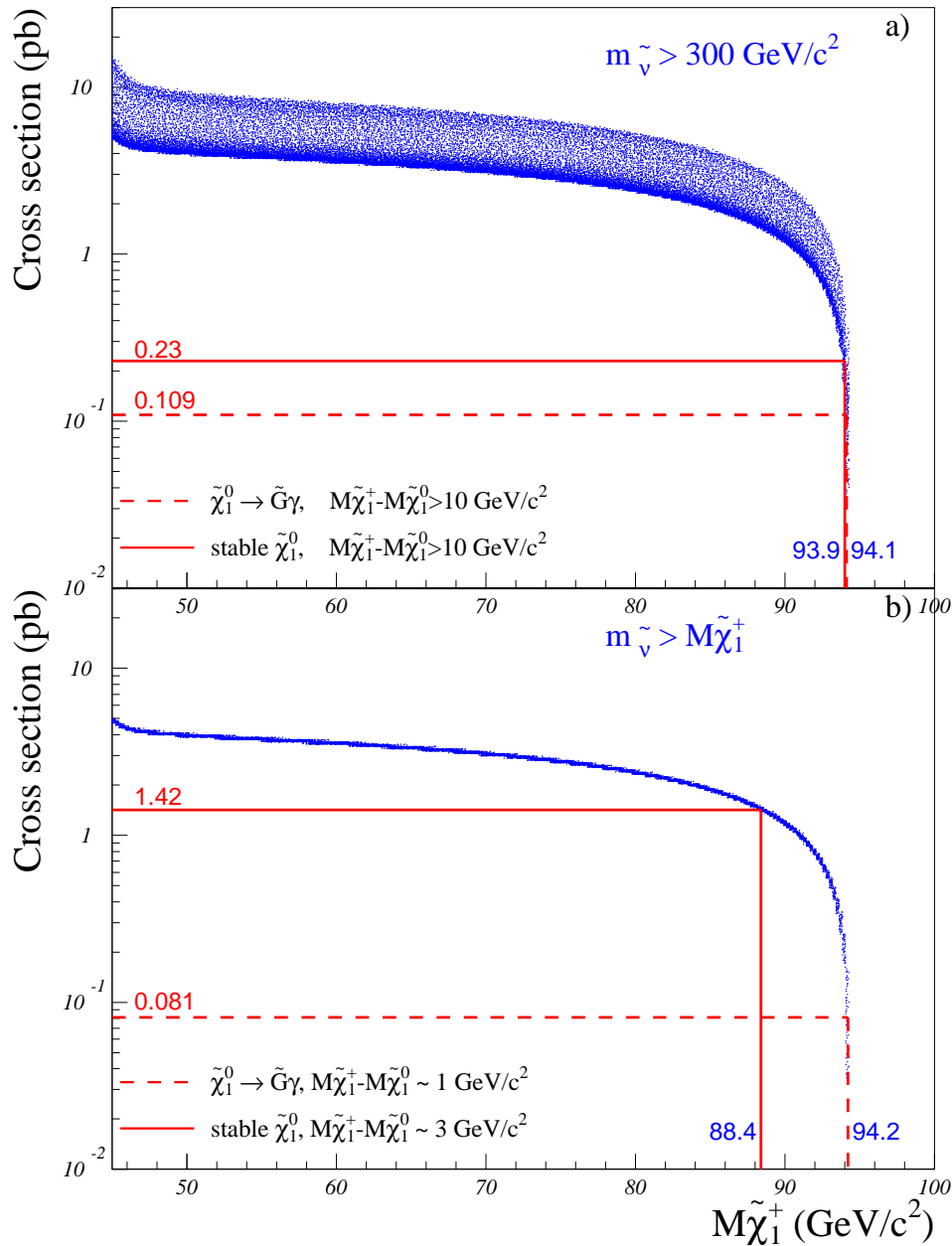
Figure 3: Expected cross-sections in pb at 189 GeV (dots) versus the chargino mass in a) in the non-degenerate case ($\Delta M > 10$ GeV/c^2) and b) the degenerate case ($\Delta M \sim 3$ GeV/c^2). The spread in the dots originates from the random scan over the parameters μ and M_2. A heavy sneutrino ($m_{\tilde{\nu}} > 300$ GeV/c^2) has been assumed in a) and $m_{\tilde{\nu}} > M_{\tilde{\chi}_1^\pm}$ in b). The minimal cross-sections below the mass limits are indicated by the horizontal lines.

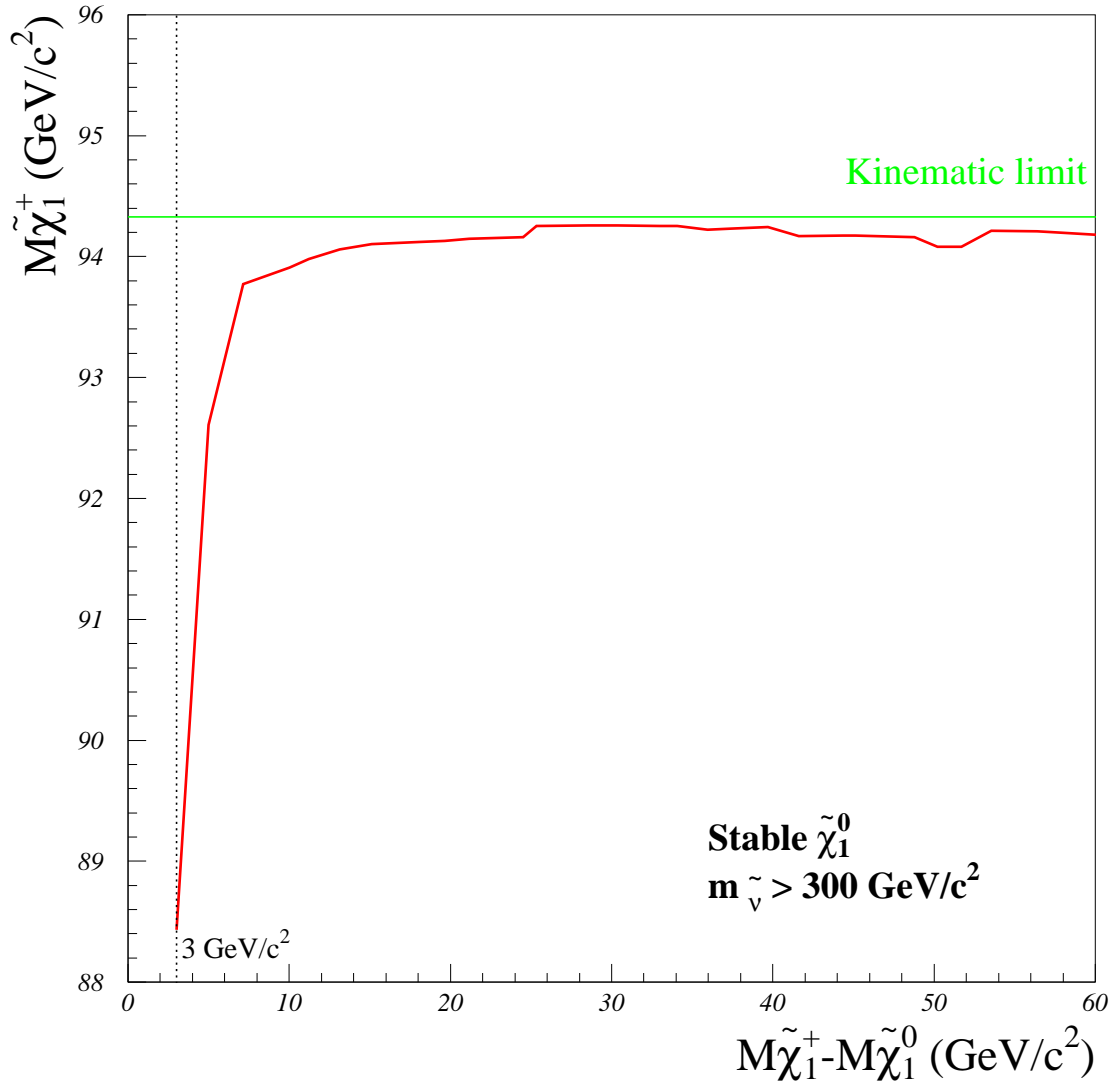# DELPHI $\tilde{\chi}_1^+\tilde{\chi}_1^-$ limits at 189 GeV

Figure 4: The chargino mass limit as function of the ΔM value under the assumption of a heavy sneutrino. The limit applies to the case of a stable $\tilde{\chi}_1^0$. The straight horizontal line shows the kinematic limit.
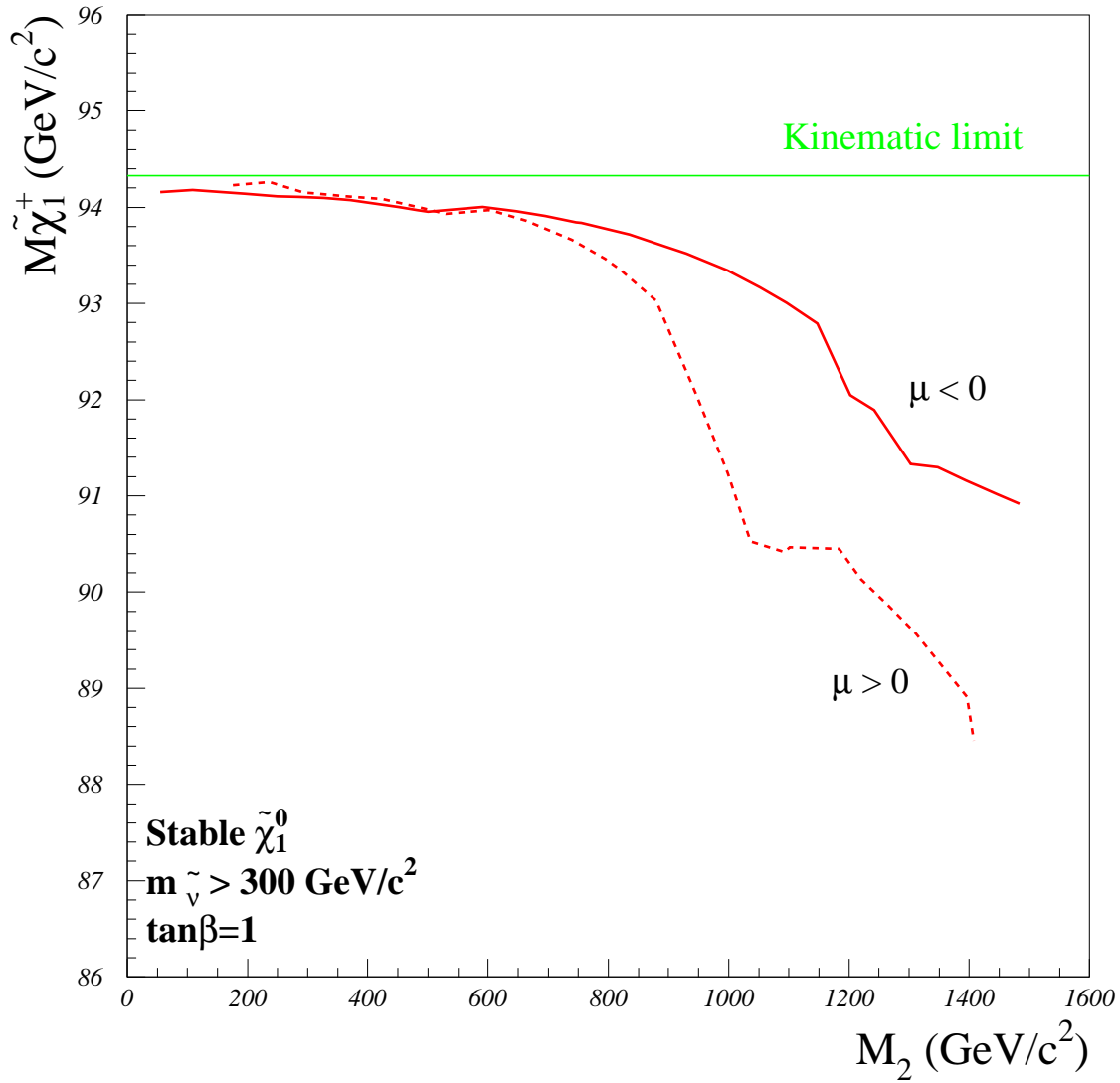
Figure 5: The chargino mass limit as function of M_2 for $\tan\beta = 1$, under the assumption of a heavy sneutrino ($m_{\tilde{\nu}} > 300\,\mathrm{GeV}/c^2$). The straight horizontal line shows the kinematic limit in the production. The limit applies in the case of a stable $\tilde{\chi}_1^0$.
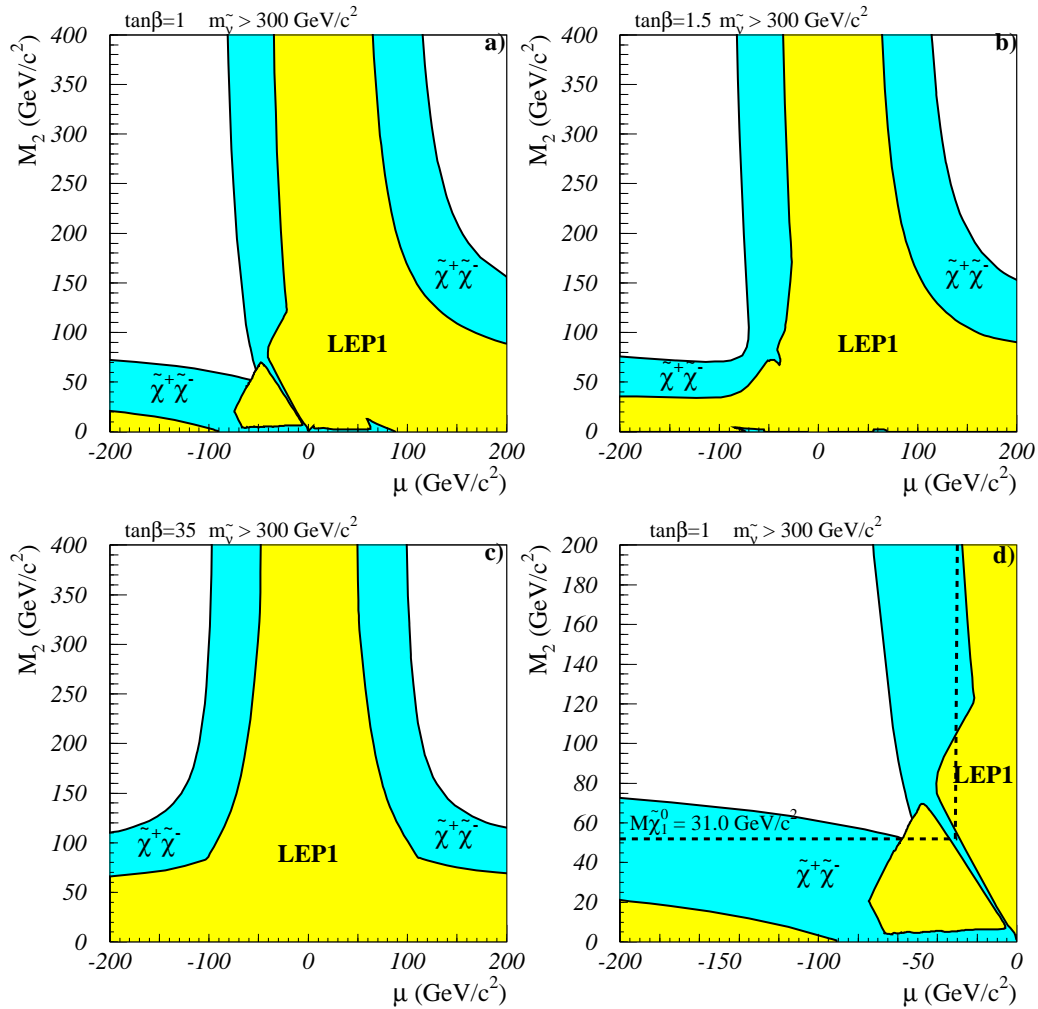
DELPHI MSSM limits at 189 GeV

Figure 6: a), b), and c), regions excluded at 95 % confidence level in the (μ, M_2) plane at $\sqrt{s} = 189$ GeV under the assumption of a heavy sneutrino for $\tan\beta = 1$, 1.5 and 35. The dark shading shows the region excluded by the chargino search and the light shaded region is the one excluded by LEP1. The constant mass curve for the LSP mass limit is shown in d) by the dashed line, for $\tan\beta = 1$.
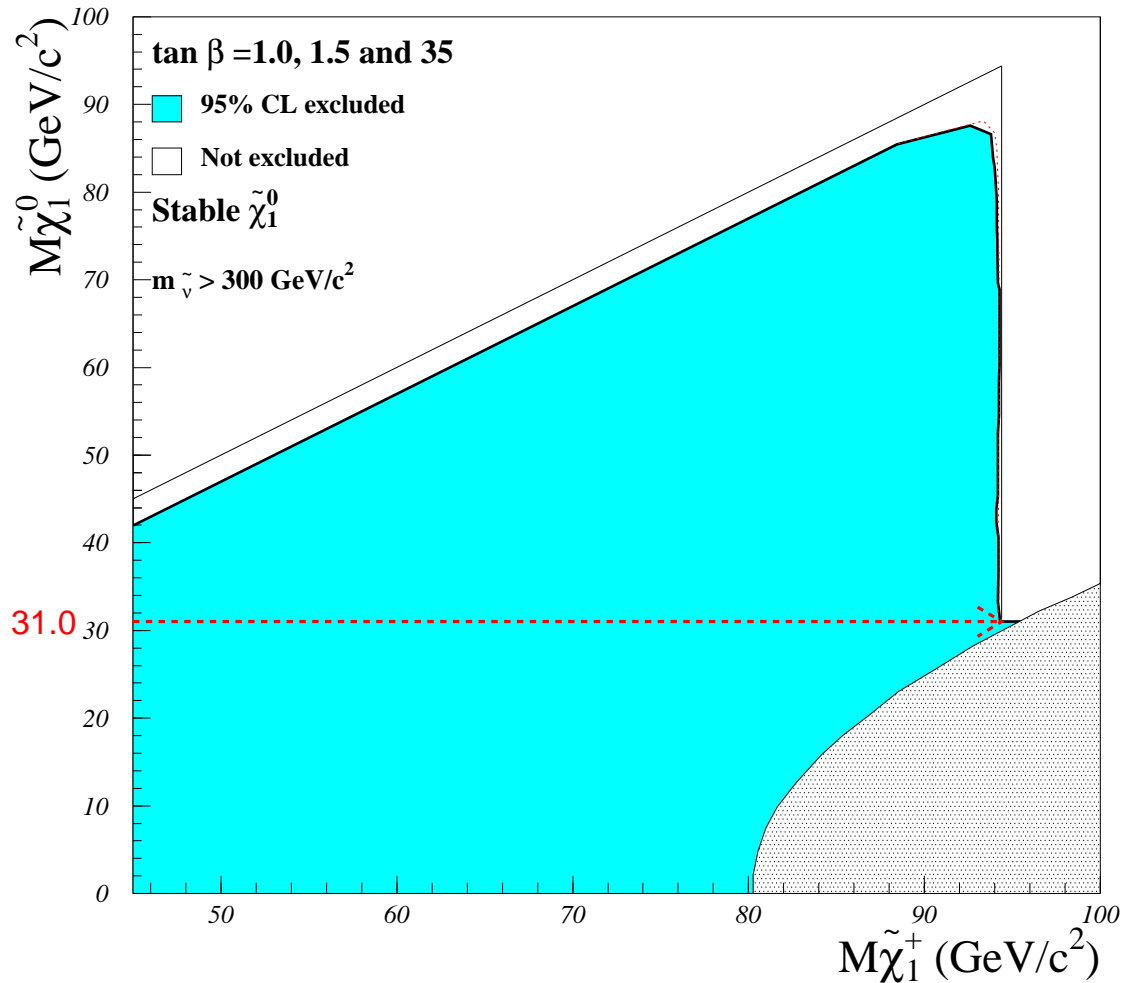
Figure 7: Region excluded at 95% confidence level in the plane of the mass of the lightest neutralino versus that of the lightest chargino under the assumption of a heavy sneutrino, for $\tan\beta = 1.0$, 1.5 and 35. The thin lines show the kinematic limits in the production and the decay. The dotted line (partly hidden by the shading) shows the expected exclusion limit. The lightly shaded region is not allowed in the MSSM. The limit applies in the case of a stable $\tilde{\chi}_1^0$. The mass limit on the lightest neutralino is indicated by the horizontal dashed line. The excluded region outside the kinematic limit is obtained from the limit on $\tilde{\chi}_1^0\tilde{\chi}_2^0$ production at the Z resonance derived from the single-photon search.

DELPHI $\tilde{\chi}^+\tilde{\chi}^-$ efficiencies (189 GeV)

Total detection efficiency

$\tilde{\chi}_1^0 \to \tilde{G}\gamma$

>45

>50

>45

>40

>35

>30

Not allowed

M($\tilde{\chi}_1^0$) (GeV/c^2)
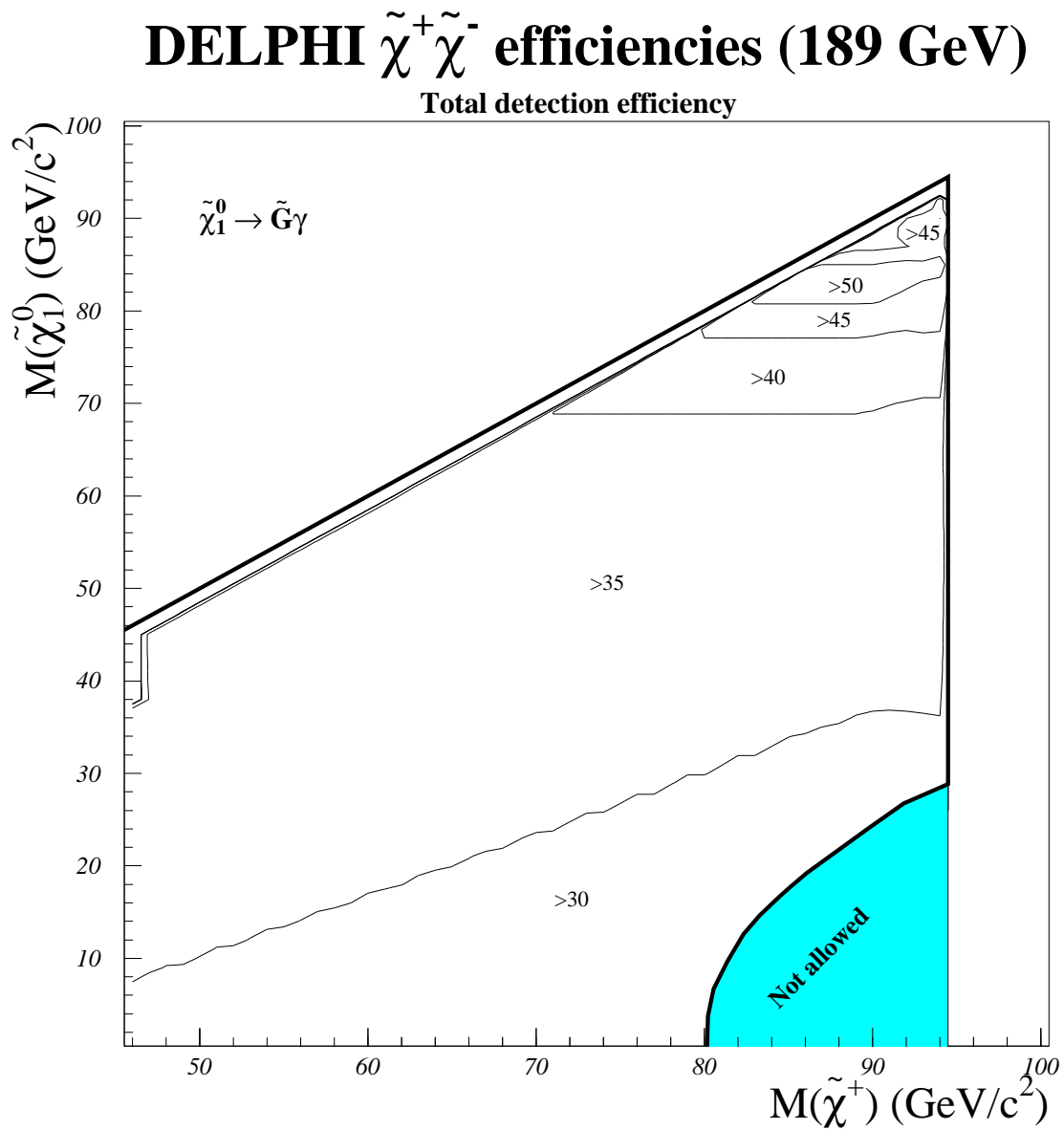
M($\tilde{\chi}^+$) (GeV/c^2)

Figure 8: Chargino pair production detection efficiency (%) at 189 GeV in the $(M_{\tilde{\chi}^\pm}, M_{\tilde{\chi}^0})$ plane. An unstable $\tilde{\chi}_1^0$ is assumed. The shaded areas are disallowed by the MSSM scheme.